Available online at www.sciencedirect.com

ScienceDirect

Procedia CIRP 111 (2022) 810–815

www.elsevier.com/locate/procedia

12th CIRP Conference on Photonic Technologies [LANE 2022], 4 – 8 September 2022, Fürth, Germany

A holistic approach for an intelligent laser beam welding architecture using machine learning for the welding of metallic bipolar plates for polymer electrolyte membrane fuel cells

Tony Weiss[a]*, Michael Kick[a], Sophie Grabmann[a], Christian Geiger[a], Lukas Mayr[a], Katrin Wudy[b], Michael F. Zaeh[a]

[a]*Technical University of Munich, TUM School of Engineering and Design, Institute for Machine Tools and Industrial Management (iwb), Boltzmannstrasse 15, 85748 Garching, Germany*

[a]*Technical University of Munich, TUM School of Engineering and Design, Professorship of Laser-based Additive Manufacturing (LBAM), Boltzmannstrasse 15, 85748 Garching, Germany*

* Corresponding author. Tel.: +49-089-289-55474; fax: +49-089-289-15555. *E-mail address:* tony.weiss@iwb.tum.de

Abstract

Laser beam welding is the state-of-the-art technology for joining micro-formed metal foils in the manufacturing of bipolar plates for proton exchange membrane fuel cells. However, the process is limited in the achievable welding speed since humping and undercut effects can occur at high feed rates. These effects significantly reduce the weld seam quality, causing scrap or subsequent failure during operation. As a result, higher manufacturing costs arise and additional quality assurance is needed. In this work, welding experiments, including a photodiode-based sensor system, were conducted on AISI 316L metal foils to evaluate the capability of this sensor for inline and online quality assurance. Based on the results, an intelligent laser beam welding architecture is proposed, representing a holistic approach for a multi-sensor-based and self-improving quality assurance system. The theoretical architecture combines a novel laser beam welding concept with different optical and acoustic sensors for determining the current weld state. It considers sensor data fusion for relevant information on the process behavior via dedicated algorithms applying deep neural networks. The approach is an idea of a predictive weld state determination for a precise and real-time capable weld seam quality assurance.

Keywords: laser beam welding; bipolar plates; fuel cells; process monitoring; sensor data fusion; machine learning

1. Introduction

In order to further advance the transition from fossil fuel-based mobility to electric mobility, innovative manufacturing processes are needed to bring new technologies into series production. The objective is to further enhance the quality and safety of components while reducing manufacturing costs. Laser beam welding is used in many applications in the field of electromobility, e.g., for contacting battery cells [1], in the production of fuel cells for hydrogen-based mobility, or energy generation. A core component of low-temperature polymer electrolyte membrane fuel cells (PEMFC) are bipolar plates. Since the production of bipolar plates accounts for approximately 20 – 30 % of the total costs of fuel cells, there is particular potential for cost and material savings in terms of manufacturing [2]. Therefore, various materials are being considered for the fabrication of bipolar plates, including metallic, non-porous graphite, and composite materials. As coated stainless-steel foils (e.g., AISI 316L) show numerous advantages over other materials, such as a high thermal and electrical conductivity as well as superior mechanical properties, their application is favored for bipolar plates [3]. Depending on the

10.1016/j.procir.2022.08.089

material and the application, the metal foils have a thickness of approx. 50 – 150 µm [3]. In order to join two metal foils in the manufacturing of bipolar plates so that they are gas-tight, laser beam welding is used as the state-of-the-art joining process. An observable process instability when welding thin metal foils is the humping effect. With the aforementioned material thicknesses, it occurs at welding speeds above 700 mm/s [4], depending on the material thickness, the welding speed, and the optical setup [5]. At high welding speeds, the melt pool velocity exceeds the welding speed, accelerating the melt pool around the keyhole [5]. Additional melt pool turbulences in back of the keyhole further accelerate the melt pool towards the weld seam center [6]. In the rear area of the melt pool, the melt jet is slowed down by solidification processes, resulting in periodic humps. Another challenge is the clamping situation, which is crucial for a reproducible positioning and achieving a zero gap between both foils [7] . With numerous sensor technologies available, there is still substantial research and development needed for applications in the field of laser material processing. Therefore, a lack of a comprehensive and qualified inline quality inspection for the welding of metallic bipolar plates was identified. For this process, one monitoring system is not sufficient to fully detect different types of defects, such as undercut, burn through, lack of fusion, and humping, as each sensor is only able to detect specific quality characteristics of the weld seam [8]. Thus, a method for combining different sensors is necessary. Existing publications and ongoing research on sensors for laser beam welding applications demonstrated that a variety of different sensor approaches are suitable for monitoring the laser beam welding process. They are used for capturing real-time information about the welding process and for detecting weld defects inside as well as on the surface of the weld seam. Using the principle of the optical coherence tomography (OCT) in a sensor, a novel tool is available to measure the keyhole depth inline [9] and to use the signal's information for a determination of the weld seam quality [10]. Since one advantage of the OCT is to directly measure the keyhole depth, the correlation between signal characteristics and the weld depth can be obtained. Another suitable method to monitor the laser beam welding process was shown by Shevchik et al. [11], who used photodiodes for the recording of different process emission wavelengths and an acoustic sensor. The signals were analyzed afterwards and served as inputs for a weld seam classification using machine learning methods. As a common approach, charge-coupled devices (CCD) [12] or thermographic cameras [13] are being applied to gather information about the welding process. Advantages are a direct recording of the weld seam surface and the detection of possible irregularities and spatter formation [14]. For the evaluation of the image and signal data of the aforementioned sensors, machine learning techniques are suitable methods to correlate the data to process characteristics and the quality of the weld seam. Guenther et al. proposed a combined application of sensors and machine learning in laser beam welding applications [15]. The focus of their research was an architecture based on Reinforcement Learning and Deep Neural Networks for processing camera image data and signals from photodiodes with the goal of implementing a process control.

2. Objectives

Several sensor systems are commercially available to monitor the laser beam welding process. In the case of joining metallic foils for the manufacturing of bipolar plates, there are no investigations concerning the combined inspection of burn trough and humping, for instance, using a photodiode-based sensor system. In the presented work, the sensor system was used for an inline and online inspection. Based on the results, a design for an intelligent inline laser beam welding architecture was derived.

3. Experimental setup

In order to investigate the suitability of a photodiode-based sensor system, the welding process was monitored using a laser welding monitor (LWM, Precitec GmbH & Co. KG, Germany, Fig. 1). The experiments were conducted with a continuous-wave (cw) multi-mode disk laser (TruDisk 1020, Trumpf SE & Co. KG, Germany) with a wavelength of 515 nm. The beam was deflected by a scanning optics (PFO20-2 TF1, Trumpf SE & Co. KG, Germany). The optical fiber of the laser beam source had a core diameter of 50 µm and the imaging ratio of the optical setup was 2.93. In this experiment, the working distance was chosen according to the focus of the laser beam, leading to a spot diameter of 150 µm.

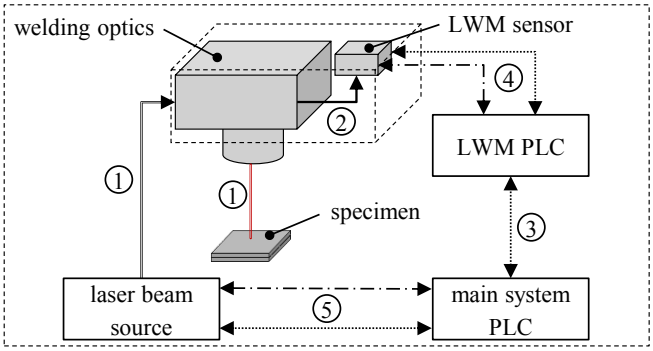

Fig. 1. Experimental setup for an overlap weld of two 80 µm stainless steel 316L foils.

Equipped with a programmable logic controller (PLC), the LWM recorded the measured signals from three photodiodes. The photodiodes measured the wavelengths 515 nm (reflection), 450 – 780 nm (plasma, green light filtered out), and 1100 – 1800 nm (temperature). As the control of the laser cell, the main system PLC processed all signals from the peripheral components. It represents the interface between the laser beam source, the optics, and the LWM. For a synchronized measurement of the process emissions, a trigger signal was generated by the main PLC at the start and end of the laser emission that started and stopped the measurement of the LWM. The three photodiodes recorded the individual signals during the welding

process with a sampling rate of 50 kHz defined by the LWM PLC. In addition, the laser power was being recorded synchronized with the mentioned signals. As a sample material, stainless steel AISI 316L was selected for the welding experiments. The chosen specimen geometry can be seen in Figure 2. Overlap welds with a length of 15 mm were performed on two metal foils with a film thickness of 80 µm each and outer dimensions of 25 mm × 25 mm. In order to achieve the highest productivity for the manufacturing of bipolar plates, the laser power was kept constant at 1 kW during the experiments, with the welding speed increased in 50 mm/s increments from 1150 to 1850 mm/s.

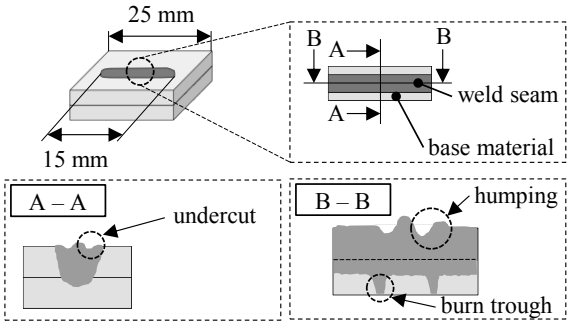

Fig. 2. Sample geometry and major weld seam defects that occurred during the experiments.

Three identical tests were performed for 15 different parameter setups, whereby the process emissions were measured inline (during welding) and online (directly after welding) by the LWM. The online measurements were performed with a laser power of only 30 W and 100 W, respectively, to compare the signal characteristics with the inline measurements without changing the weld seam properties after the process.

For the inline and online measurement, the recorded process emissions were evaluated offline after the experiments using Matlab R2021b. Since the signals were saved as time series data, a transformation was performed to synchronize them to the corresponding weld seam positions. This allows the sensor data to be subsequently mapped directly to an image of the weld seam, recorded by a laser scanning microscope (LSM).

4. Results and discussion

As a result, five major areas within the investigated parameter range were distinguished, based on the occurring external weld seam properties and defects (Table 1).

Table 1. Identified weld seam properties and major defects on the seam surface for the investigated parameter range

ID	occurred weld defect(s)	feed rate (*mm/s*)
1 – 4	occasional humping without holes, strong burn-in on the backside	1150 – 1300
5 – 7	occasional humping without holes, slight burn-in on the backside	1350 – 1450
8 – 12	increased strong humping with imperfections and holes	1500 – 1700
13 – 14	occasional humping, start of lack of fusion	1750 – 1800
15	lack of fusion	1850

In Figure 3, the LWM signals are shown together with an LSM image of the corresponding weld seam surface for one of the specimens welded with 1700 mm/s. Welding was performed in positive x-direction. The sample was chosen, because a strong humping effect with subsequent holes is clearly visible on the specimen's surface. After processing the data, no anomaly was identified within the inline measured signals, which indicated the occurrence of humping. The emissions recorded by the photodiodes originated from the process zone. As the humping appeared in back of the process zone in the feed direction, the emitted radiation from this area could not be detected with the used sensor setup. Therefore, the online measurements were conducted while the welded foils were still clamped down. In contrast to the inline measurement, the online recorded data associated to 100 W laser power showed clear peaks in the signal waveforms for the plasma, temperature, and reflection signal in the areas where humping occurred (Fig. 3).

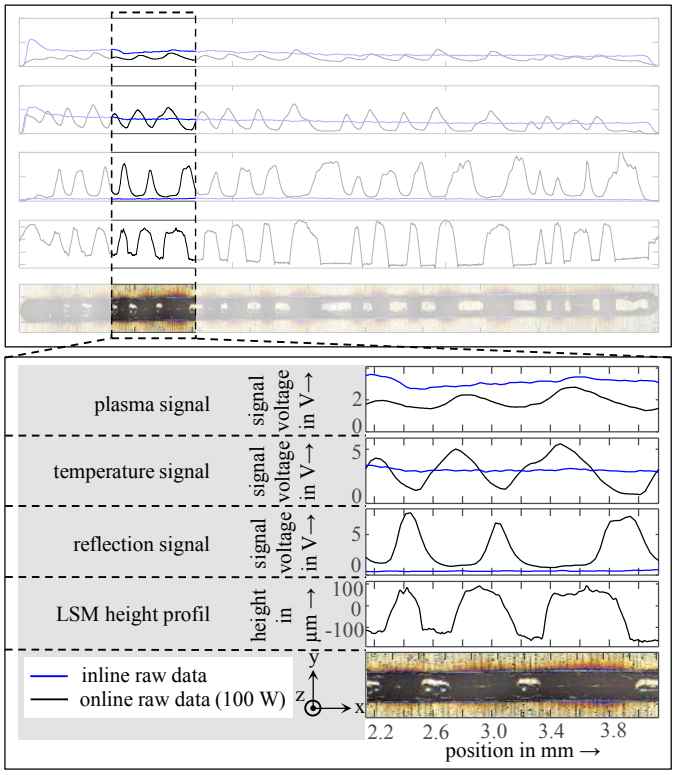

Fig. 3. Inline and online measured LWM signals of a sample (P = 1000 W, v = 1700 mm/s) correlated to the corresponding weld seam.

The reflection signal has approximately the same signal curve as the height profile extracted from the LSM analysis, whereas the temperature and plasma signals are opposed to the reflection signal. In areas with humping, a peak in the reflection signal was visible. Consequently, the temperature and plasma signals have a local minimum in the same segment. For all three signals, the time-shifted appearance of peaks with regard to the local seam topography was characteristic. As for the reflection signal, the peaks occurred with a time-shift (not consistent) after a hump in the seam surface. The peaks in the temperature and plasma signal occurred with a time-shift after a hole in the seam surface, respectively. Additionally, the temperature and plasma signal curves were nearly identical, while the plasma

signal voltage was lower. A further analysis showed that the three signal voltages (photodiodes) of the mentioned 100 W dataset were higher than the corresponding measurement associated to 30 W laser power, see Fig. 4. The differences can be explained by the resulting higher process emissions, which originated from the process zone when the laser power was set to 100 W.

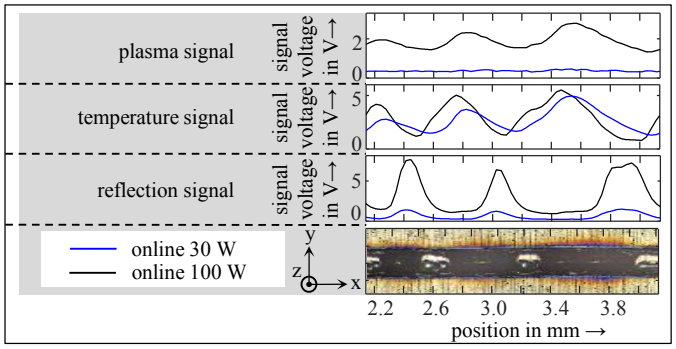

Fig. 4. Comparison of the online measured LWM signals of an already welded sample (P = 1000 W, v = 1700 mm/s) carried out with 30 W and 100 W processing laser power.

In addition, the LWM data of the samples welded with 1850 mm/s (lack of fusion between top and bottom foil) were compared with the datasets representing a successful weld in the range of 1150 mm/s – 1800 mm/s. In order to analyze the measurements, boxplots were used to visualize the inline recorded data of the plasma, temperature, and reflection signal, respectively. With this method, the statistical distribution of the data points is given (cf. Fig. 5). The central red mark on each box indicates the median, whereby the bottom and top edges of the box indicate the lower (25th percentile) and upper (75th percentile) quartiles. The whisker length was set to 1.5 times the interquartile range. The temperature and the reflection signals of the welding conducted with a corresponding welding speed of 1850 mm/s showed no distinct relationship between anomalies in the signal and the resulting lack of fusion of the two stainless-steel foils.

However, when looking at the boxplots of the plasma signals in Figure 5, the median values are slightly ascending with an increasing welding speed and a decreasing weld depth. For the samples welded with 1850 mm/s, the according boxplot shows a sudden decrease in the median value with a simultaneous increase in the interquartile range (1.68 V). Additionally, the distance of the upper (5.969 V) and lower (0.171 V) adjacent value increases significantly compared to the previous boxplots of the successfully welded samples. The adjacent values are the upper and lower limit of the data points that are not outliers. With the associated signal behavior as a basis, it is assumed that the changes in the statistical values are an indicator for the lack of fusion between top and bottom foil during welding. Therefore, a threshold value for detecting the welding defect will be defined in further work based on a statistical signal evaluation. At this point, further experiments are necessary to validate the identified signal behavior extensively as well as a transfer of the results to a signal analysis for burn-through effects during welding.

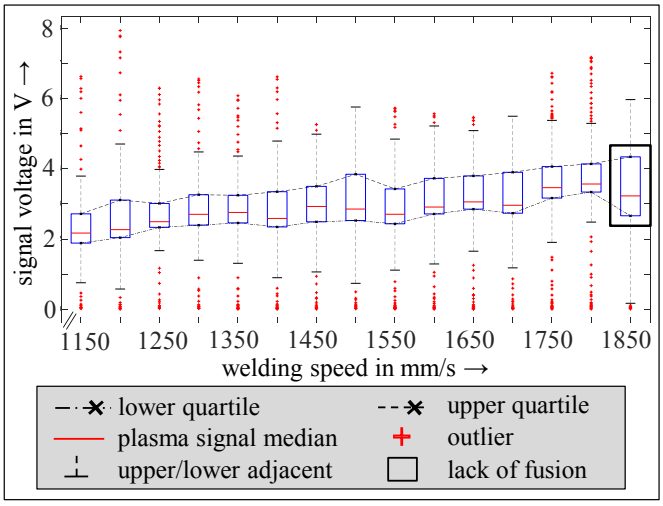

Fig. 5. Boxplots of the inline recorded plasma signals for the investigated welding parameters.

5. Design of an intelligent laser beam welding architecture

The results of the experiments showed that a photodiode-based system can detect single process defects, such as humping (online) or lack of fusion (inline). These results can contribute to an intelligent laser beam welding architecture for the welding of metallic bipolar plates which is presented as a concept within this paper. The core of this system is the integrated adaptive data processing method using machine learning algorithms for the interpretation of sensor signals. Additionally, a sensor data fusion approach as a basis for an inline weld seam quality prediction is derived to increase process reliability. The goal is to provide redundant information for a 100 % inline quality assurance to substitute complex quality tests. For the welding of metallic bipolar plates, the available sensors are not yet qualified extensively. In the architecture shown in Figure 6, four sophisticated sensors are combined to monitor different aspects of the process. These sensors are chosen to guarantee redundancy with respect to the process monitoring of all relevant phenomena, such as humping and burn through. Additionally, the selected sensors are capable of detecting weld seam properties and possible weld defects, as outlined in section 1.

5.1. Process and sensor level

During welding, optical and acoustic process emissions are generated (Fig. 6, section A – process level), for which the corresponding sensors are suitable. Section B of Figure 1 reflects the sensor level, which contains a photodiode-based sensor system, an OCT sensor, a high-speed (thermographic) camera, and an optical microphone. While the OCT system directly measures the keyhole depth [9] and is therefore suitable for detecting burn throughs or insufficient penetration, the photodiodes record emissions from the process zone, for example, in the visible, near-infrared, and infrared spectrum. It is assumed that the time series data can be used for detecting gaps between two foils or burn throughs as well. Furthermore, the OCT signal can be analyzed to determine the keyhole geometry [16] and seam internal weld defects, such as pores [17]. A high-speed

camera as the third sensor records the surface of the melt pool during the process. With image processing, it is possible to visualize the formation of spatters and near-surface pores. Additionally, the direct inspection of the weld seam surface via Deep Neural Networks allows for the detection of humping as one of the major seam defects and reasons for scrap in the welding of bipolar plates. Instead of a camera for the visible wavelengths, a thermographic camera may be used as an alternative to detect process emissions originating from the keyhole as a redundancy to the recorded photodiode signals. As the optical microphone is capable of sampling with a frequency of up to several MHz, the recording of different process characteristics is superior compared to the described optical sensor systems. Existing publications showed that acoustic process emissions during laser material processing can be used to detect the formation of spatters [18], [19]. It is assumed that an optical microphone is therefore capable of detecting the occurrence of the humping and the detachment of larger spatters and melt formations as well. This hypothesis will be subject to further work. As a result, the individual capabilities of the sensors will complement each other to form an overall and holistic monitoring system.

5.2. Data and prediction level

Section C (Fig. 6) displays the data level in which the signals are downsampled within several processing steps as a basis for the quality prediction (Fig. 6, section C1). Section C1 contains individual wavelet transformations for the acoustic signatures and the occasionally highly scattered OCT depth signal to derive relevant features, such as included frequencies or statistical parameters, the standard deviation, for instance. The photodiode signals can be pre-processed through a percentile filter with a moving average window. For pre-processing the camera images, different image correction methods, such as denoising and sharpening, are applied. The following two paths, C2.1 and C2.2, contain the algorithms and pre-trained artificial neural networks (ANN) for the quality prediction. Their basic procedures differ fundamentally. On path C2.1, a feature fusion is performed as the next step after pre-processing. After aligning and synchronizing the data, a convolutional neural network (CNN) combines the time series data and the 2D image data via a hybrid architecture, representing a feature level fusion [20]. Based on the combined information, the weld seam (part) is classified by a second ANN. On path C2.2, the classification is performed individually for each sensor first with appropriate ANNs. They are applied to the time series data, if suitable, to detect trends in the signal behavior for overlapping segments. In the following step, the four predictions are combined, and using an ANN, the final prediction for the current segment is determined. This approach represents a decision level fusion [20]. On the prediction level (Fig. 6, section D), the overall weld seam quality prediction is performed by merging the single classified segments and displaying the quality of the entire weld seam. Via active (machine) learning, the decisions made by the ANNs are verified. False positive or false negative classifications will be identified. They are used for re-training the implemented neural networks to further increase the classification accuracy.

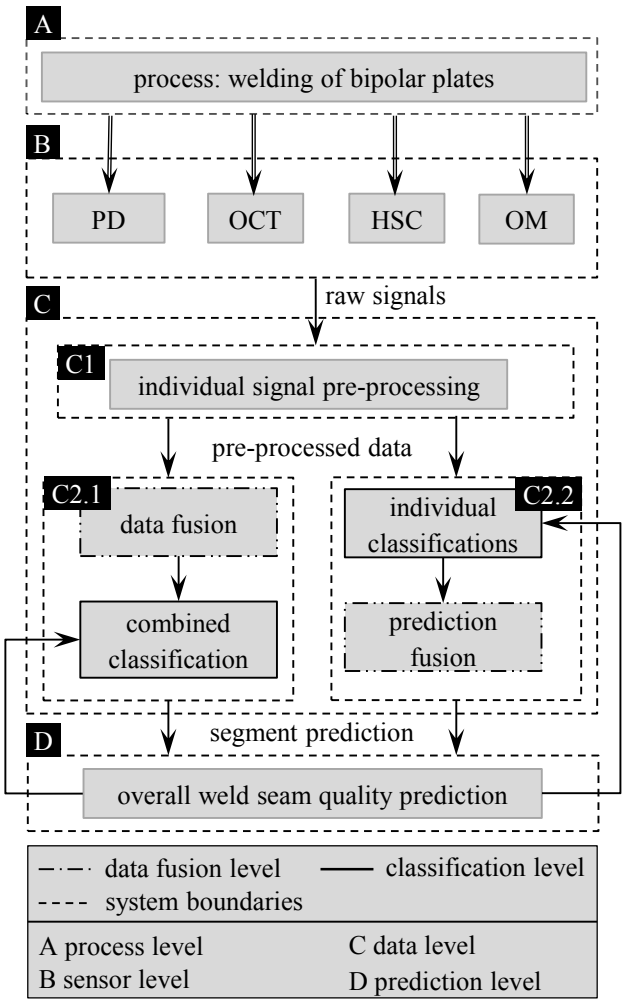

Fig. 6. Intelligent laser beam welding architecture combining different sensor approaches and applying sensor data fusion; PD: photodiodes, OCT: optical coherence tomography sensor, HSC: high-speed camera, OM: optical microphone

6. Conclusion

In this work, the results of laser beam welding experiments using green laser radiation for the joining of two 80 µm stainless-steel AISI 316L foils were presented. The process emissions were measured inline first via a photodiode-based laser welding monitor (LWM). It was shown that no anomalies in the inline signal correlated to the humping effect could be identified in the data. However, the signal analysis showed a possible relationship between statistical signal values and the weld state, indicating a lack of fusion. Thus, a determination of the weld depth based on the plasma signal needs to be investigated in detail in a further study. Additionally, online measurements with 30 W and 100 W processing laser power were performed. Based on a signal analysis, a relationship between the occurrence of humping and the signal characteristics was identified for the online measurements of the LWM sensor. Especially for the reflection signal, the correlation to the weld seam surface was significant. With the shown procedure, it is possible to implement an online measurement strategy based on the LWM to detect humping. Deploying a sensor with a higher sampling rate, the online measurement can be performed even faster after the welding process.

Since a single sensor can only detect specific weld defects, an intelligent laser beam welding architecture and its implementation were proposed in detail together with a novel sensor data fusion concept. This architecture aims on redundant information about the welding process to reliably predict the weld seam quality.

Concerning the LWM, a further study will investigate in detail the effects of a burn-through on the signal behavior within an extended validation based on the assumptions made. An increase in the parameter range with respect to a variation of the laser power will be included as well as experiments regarding the detectability of other weld seam properties and defects using the LWM sensor.

For the intelligent laser beam welding architecture, the remaining sensors need to be investigated thoroughly concerning the suitability for measuring weld seam properties and defects for the underlying application.

References

[1] Brand MJ, Schmidt PA, Zaeh MF, Jossen A. Welding techniques for battery cells and resulting electrical contact resistances. Journal of Energy Storage 2015;1: pp. 7 – 14.

[2] James BD, Huya-Kouadio JM, Houchins C. Bipolar plate cost and issues at high production rate. Southfield, Michigan; 2017.

[3] Song Y, Zhang C, Ling C-Y, Han M, Yong R-Y, Sun D, Chen J. Review on current research of materials, fabrication and application for bipolar plate in proton exchange membrane fuel cell. International Journal of Hydrogen Energy 2020;45: pp. 29832 – 29847.

[4] Haddad E, Chung WS, Katz O, Helm J, Olowinsky A, Gillner A. Laser micro welding with fiber lasers for battery and fuel cell based electromobility. Journal of Advanced Joining Processes 2022;5: pp. 100085.

[5] Hügel H, Graf T. Laser in der Fertigung: Grundlagen der Strahlquellen, Systeme, Fertigungsverfahren. 3rd ed. Wiesbaden: Springer Vieweg; 2014.

[6] Fuhrich T. Marangoni-Effekt beim Laserstrahltiefschweißen von Stahl. Stuttgart, Univ., Diss. Muenchen: Herbert Utz Verlag; 2005.

[7] Grabmann S, Tomcic L, Zaeh MF. Laser beam welding of copper foil stacks using a green high power disk laser. Procedia CIRP 2020;94: pp. 582 – 586.

[8] Stritt P, Boley M, Heider A, Fetzer F, Jarwitz M, Weller D, Weber R, Berger P et al. Comprehensive process monitoring for laser welding process optimization 2016: pp. Q1 – Q10.

[9] Schmoeller M, Stadter C, Liebl S, Zaeh MF. Inline weld depth measurement for high brilliance laser beam sources using optical coherence tomography. Journal of Laser Applications 2019;31: pp. 22409.

[10] Stadter C, Schmoeller M, Rhein L von, Zaeh MF. Real-time prediction of quality characteristics in laser beam welding using optical coherence tomography and machine learning. Journal of Laser Applications 2020;32: pp. 22046.

[11] Shevchik SA, Le-Quang T, Farahani FV, Faivre N, Meylan B, Zanoli S, Wasmer K. Laser Welding Quality Monitoring via Graph Support Vector Machine With Data Adaptive Kernel. IEEE Access 2019;7: pp. 93108 – 93122.

[12] Mayr A, Lutz B, Weigelt M, Glabel T, Kibkalt D, Masuch M et al. 2018 8th International Electric Drives Production Conference (E|DPC): 4 and 5 December 2018, Schweinfurt, Germany proceedings. Piscataway, NJ: IEEE; 2018.

[13] Schaumberger K, Beck M, Saffer J, Kaufmann F, Ermer J, Roth S, Schmidt M. Improving process reliability by means of detection of weld seam irregularities in copper via thermographic process monitoring. Procedia Manufacturing 2019;36: pp. 58 – 63.

[14] Haubold MW, Zaeh MF. Real-time spatter detection in laser welding with beam oscillation. Procedia CIRP 2019;79: pp. 159 – 164.

[15] Guenther J, Pilarski PM, Helfrich G, Shen H, Diepold K. Intelligent laser welding through representation, prediction, and control learning: An architecture with deep neural networks and reinforcement learning. Mechatronics 2016;34: pp. 1 – 11.

[16] Stadter C, Kick MK, Schmoeller M, Zaeh MF. Correlation analysis between the beam propagation and the vapor capillary geometry by machine learning. Procedia CIRP 2020;94: pp. 742 – 747.

[17] Schmoeller M, Stadter C, Kick MK, Geiger C, Zaeh MF. A Novel Approach to the Holistic 3D Characterization of Weld Seams-Paving the Way for Deep Learning-Based Process Monitoring. Materials (Basel) 2021;14.

[18] Schmidt L, Römer F, Böttger D, Leinenbach F, Straß B, Wolter B, Schricker K, Seibold M et al. Acoustic process monitoring in laser beam welding. Procedia CIRP 2020;94: pp. 763 – 768.

[19] Gutknecht K, Cloots M, Sommerhuber R, Wegener K. Mutual comparison of acoustic, pyrometric and thermographic laser powder bed fusion monitoring. Materials & Design 2021;210: pp. 110036.

[20] Hall DL, Llinas J. An introduction to multisensor data fusion. Proc. IEEE 1997;85: pp. 6 – 23.